We are IntechOpen,
the world's leading publisher of
Open Access books
Built by scientists, for scientists

4,800

Open access books available

122,000

International authors and editors

135M

Downloads

Our authors are among the

154

Countries delivered to

TOP 1%

most cited scientists

12.2%

Contributors from top 500 universities

WEB OF SCIENCE™

Selection of our books indexed in the Book Citation Index
in Web of Science™ Core Collection (BKCI)

Interested in publishing with us?
Contact book.department@intechopen.com

Numbers displayed above are based on latest data collected.
For more information visit www.intechopen.com

State-Of-The-Art Methods for the Numerical Simulation of Aortic BMHVs

Sebastiaan Annerel[1], Tom Claessens[2], Peter Van Ransbeeck[2],
Patrick Segers[3], Pascal Verdonck[3] and Jan Vierendeels[1]
[1]Department of Flow, Heat and Combustion Mechanics, Ghent University,
[2]Department of Mechanics, University College Ghent,
[3]IBiTech-bioMMeda, Ghent University,
Belgium

1. Introduction

Since the first clinical implantation of an artificial aortic valve by Dr. Charles A. Hufnagel in 1952 (Hufnagel et al., 1954), the use of such prostheses has gained strong interest and has become a routine treatment for severe heart valve failure. During the past 60 years, various mechanical heart valve designs have been developed for use in both aortic and mitral positions (Butany et al., 2003; Aslam et al., 2007). Nowadays, bileaflet mechanical heart valves (BMHVs) are widely preferred for aortic valve replacement because of their long lifespan. However, current BMHVs still induce pannus and thromboembolism, among other undesired side effects, which are believed to be due to non-physiological flow and turbulence generated by the valve leaflets (Sotiropoulous & Borazjani, 2009).

One way to gain insight into the dynamics of a BMHV in order to improve its design is by experimental testing (Grigioni et al., 2004). Usually, *in vitro* testing is used, in which the functioning of the valve is assessed, for example, by using Doppler echocardiography (Dumont et al., 2002; Verdonck et al., 2002) or by visualizing the temporal and spatial flow field through velocimetry, like the laser Doppler anemometry (LDA) technique (Browne et al., 2000; Akutsu et al., 2001) or the particle image velocimetry (PIV) technique (Browne et al., 2000; Kaminsky et al., 2007). Also, the spectrum of the valve noise can be analyzed, as is done, for example, in Masson & Rieu (1998). Experimental *in vivo* testing is another option, using echocardiography and Doppler ultrasound to investigate the behavior of the valve after implantation in human patients (Bech-Hanssen, 2001; Aslam et al., 2007; Aljassim et al., 2008; Zogbi et al., 2009) or in animals (Yin et al., 2006).

Numerical ("*in silico*") methods can provide an alternative way to obtain relevant and detailed information for valve design optimization, since they are capable of solving the valve dynamics with a high degree of resolution in time and space (Kelly et al., 1999; Grigioni et al., 2004; Yoganathan et al., 2005; Dasi et al., 2009; Sotiropoulous & Borazjani, 2009). Moreover, they are considerably less time-consuming and less expensive during the research and development phase compared with experimental testing (Dasi et al., 2009) and are, therefore, particularly efficient for sensitivity studies (Verdonck, 2002). Unfortunately, the numerical simulation of a BMHV is a complex fluid-structure interaction (FSI) problem

because the movement of the leaflets strongly interacts with the surrounding fluid motion; therefore, the equilibrium at the fluid-structure interface needs to be taken into account.

In this chapter, a review of numerical FSI methods for BMHVs is given. Subsequently, the general dynamics and flow fields of BMHVs are discussed and illustrated by numerical simulations. This flow field typically consists of three jets. Furthermore, the design optimization challenges are described. High-flow-velocity gradients give rise to high shear stresses that can induce blood damage (Yoganathan et al., 2004). Therefore, the blood damage is discussed. The flow through the hinge region is of special interest. Finally, the cavitation phenomenon in BMHVs is discussed, because it can induce blood damage as well as structural failure (due to pitting and erosion).

2. A review of FSI methods to simulate the dynamics of a BMHV

When numerically simulating a BMHV, three problems need to be solved, namely the structural problem, the flow problem, and the interaction of the fluid and the structure at the fluid-structure interface. In the following, each of these three problems is discussed in detail.

Since the leaflets of a BMHV have a small moment of inertia and are very stiff, they are usually assumed to be rigid. A BMHV can thus be modeled as a rigid casing in which two separate rigid leaflets rotate around their hinge axes (see Fig. 1). Because the position of each rigid leaflet is solely determined by its opening angle, the bileaflet valve has two degrees of freedom.

Fig. 1. View on the ATS Open Pivot™ Standard Heart Valve with leaflets (marked in black) in the open position. The casing is visible (in white) with the blocking mechanism at the hinges

The movement of a rigid leaflet i is governed by Newton's Second Law, which states that the (structural) moment $M_{s,i}$ about its rotation axis must be in equilibrium with the product of its moment of inertia I_i and its angular acceleration $\ddot{\theta}_{s,i}$. For two leaflets, this results in the following two equations:

$$\begin{cases} M_{s,1} = I_1 \cdot \ddot{\theta}_{s,1} \\ M_{s,2} = I_2 \cdot \ddot{\theta}_{s,2} \end{cases} \tag{1}$$

Secondly, the blood flow through the valve is calculated, which is governed by the conservation of mass and the Navier-Stokes equations. For the unsteady flow of an incompressible fluid, the differential equations to be solved are given by:

$$\nabla \cdot \vec{v} = 0 \tag{2a}$$

$$\rho \frac{\partial \vec{v}}{\partial t} + \rho \nabla \left(\vec{v}\vec{v} \right) = -\nabla p + \mu \nabla^2 \vec{v} + \rho \vec{g} \tag{2b}$$

(Hirt et al., 1997; Donea et al., 2004), in which $\vec{v}$ = flow velocity vector, ρ = fluid density, t = time, μ = dynamic viscosity and p = pressure. In the case of blood flow through a BMHV, it is usually assumed that the hinge axis is in the direction of gravity. Thus, the gravity has no effect on the moment about the hinge axis (Sotiropoulos et al., 2009) and, therefore, its influence (last term in Equation (2b)) is neglected.

Computational fluid dynamics (CFD) are used to solve Equation (2) for the entire fluid domain. From the resulting flow field, the pressure and viscous forces at the fluid-structure interface are derived. These forces are integrated at the fluid-structure interface giving the pressure and viscous moment $M_{f,i}$ about the hinge axis acting on the interface.

Finally, the (kinematic and dynamic) equilibrium equations at the fluid-structure interface need to be solved. The kinematic equilibrium states that the angular position of the fluid at the fluid-structure interface (i.e. $\theta_{f,i}$) should be equal to the angular position of the structural leaflet at the interface (i.e. $\theta_{s,i}$):

$$\begin{cases} \theta_{f,1} = \theta_{s,1} \\ \theta_{f,2} = \theta_{s,2} \end{cases} \tag{3}$$

Dynamic equilibrium also needs to be achieved. When the hinges of the valve are modeled as frictionless, the structural moment $M_{s,i}$ acting on each leaflet i should be equal to the pressure and viscous moment exerted by the flow, indicated by $M_{f,i}$:

$$\begin{cases} M_{f,1} = M_{s,1} \\ M_{f,2} = M_{s,2} \end{cases} \tag{4}$$

or with Equation (1):

$$\begin{cases} M_{f,1} = I_1 \cdot \ddot{\theta}_{s,1} \\ M_{f,2} = I_2 \cdot \ddot{\theta}_{s,2} \end{cases} \tag{5}$$

Both equations of equilibrium at the fluid-structure interface are solved using FSI methods. The subscripts s and f in Equation (5) are left out from here on. In the following, the pressure and viscous moment $M_{f,i}$ and the structural acceleration $\ddot{\theta}_{s,1}$ will thus respectively be referred to as "the moment M_i" and "the angular acceleration $\ddot{\theta}_i$". With this change in notation, Equation (5) becomes:

$$\begin{cases} M_1 = I_1 \cdot \ddot{\theta}_1 \\ M_2 = I_2 \cdot \ddot{\theta}_2 \end{cases} \tag{6}$$

In the remainder of this section, classifications of FSI methods used in literature to simulate a BMHV will be made, and the characteristics of each of the mentioned methods will be explained.

2.1 Fixed grid techniques versus moving grid techniques

A first classification concerns the kinematical description of the domain. For the structural problem, the motion is usually described by the Lagrangian method, where the computational grid moves with the material velocity. This is in contrast to a fluid domain, in which the motion is generally described by the Eulerian method and, therefore, the computational grid does not deform. In case of FSI, both methods can be combined in several approaches in order to describe the motion of the domain.

One approach is the "fixed grid" method, in which an immersed structure is allowed to "fictitiously" move through the Eulerian fluid grid in a Lagrangian way. The influence of the structure boundary on the fluid outside the structure is calculated by introducing body force sources into the Navier-Stokes equations, while keeping the velocity of the fictitiously overlapped fluid coupled to the structural velocity. Since the fluid grid is fixed, there is no need for remeshing and grid adaption. However, because the fluid-structure interface is not necessarily aligned with the spatial discretization and the data are, as such, interpolated, the flow field (and thus shear stresses) at this interface is not accurately calculated. Several fixed grid methods have been developed, such as the immersed boundary (IB) method, first proposed by Peskin (1972) for the simulation of heart valves. Borazjani et al. (2008) used the sharp interface CURVIB-method for simulating a BMHV. Other IB techniques were developed and used by Tai et al. (2007), De Tullio et al. (2009) and Xia et al. (2009). Also, the fictitious domain (FD) method can be used to simulate flexible heart valves (De Hart et al., 2000, 2003; Diniz dos Santos et al., 2008; Astorino et al., 2009). This fixed grid method uses Lagrange multipliers to impose the kinematic constraints. Van Loon et al. (2004) improved the accuracy of the FD method at the fluid-structure interface by proposing a local fluid grid adaption at the structure boundary.

Another approach is to use the arbitrary Lagrangian-Eulerian (ALE) method for the fluid domain. In this "moving grid" method, the fluid grid motion is driven by the motion of its boundaries, which are typically common boundaries of the moving fluid domain and the moving structure. This method introduces a fluid grid velocity $\vec{v}_g$ into the flow equations. When integrating Equation (2) over a fluid volume V, of which the surface S is moving with grid velocity $\vec{v}_g$ and has outward normal $\vec{n}$, Equation (2) becomes:

$$\frac{\partial}{\partial t}\int_V dV + \int_S \left(\vec{v}-\vec{v}_g\right)\cdot\vec{n}\,dS = 0 \qquad (7a)$$

$$\frac{\partial}{\partial t}\int_V \rho\vec{v}\,dV + \int_S \rho\vec{v}\left(\vec{v}-\vec{v}_g\right)\cdot\vec{n}\,dS = -\int_S p\vec{n}\,dS + \int_S \mu\left(\nabla\vec{v}+\left(\nabla\vec{v}\right)^T\right)\cdot\vec{n}\,dS \qquad (7b)$$

When $\vec{v}_g = \vec{v}$, this results in a purely Lagrangian description. When $\vec{v}_g = \vec{0}$, a purely Eulerian description is recovered. Moreover, the fluid grid velocity is called "arbitrary" because it does not have to correspond to the fluid velocity. However, when the grid deformation becomes too large, as is the case with BMHVs, this could deteriorate the grid quality. Therefore, local remeshing is needed between time-steps. The main advantage of

the ALE approach is its accuracy, because the grid is aligned with the fluid-structure interface. However, the use of remeshing (and thus interpolation) introduces artificial diffusivity and can become expensive for complex three-dimensional geometries. Several studies have used the ALE approach to simulate the dynamics of the ATS Open Pivot™ Standard Heart Valve (Dumont et al., 2005, 2007), the St. Jude Medical™ BMHV (Penrose et al., 2002; Redaelli et al., 2004; Dumont et al., 2007; Guivier et al., 2007, 2009; Nobili et al., 2007, 2008; Choi et al., 2009; Hong et al., 2009), and other valve types (Makhijani et al., 1997; Vierendeels et al., 2005, 2007; Bang et al., 2006; Morsi et al., 2007).

2.2 Monolithic solver versus partitioned solver

Secondly, one can classify each FSI simulation by using a partitioned solver or a monolithic solver. In the monolithic approach, the entire FSI problem is simultaneously simulated by one solver.

This is in contrast to the partitioned approach, which solves the flow and the structural problem separately and, therefore, mostly uses different specialized solvers. The partitioned approach is used to simulate heart valves in Makhijani et al. (1997), Penrose et al. (2002), Redaelli et al. (2004), Dumont et al. (2005, 2007), Vierendeels et al. (2005, 2007), Bang et al. (2006), Guivier et al. (2007, 2009), Nobili et al. (2007, 2008), Morsi et al. (2007), Tai et al. (2007), Borazjani et al. (2008), Diniz dos Santos et al. (2008), Astorino et al. (2009), Choi et al. (2009), De Tullio et al. (2009), Hong et al. (2009) and, finally, Xia et al. (2009). In order to obtain the interaction between the fluid and the structure, data exchange at the fluid-structure interface and a coupling scheme between the separated solvers are needed. Unfortunately, not every coupling scheme converges quickly. The instability of coupling schemes without relaxation is analytically explained in Vierendeels et al. (2005) and Borazjani et al. (2008) for the case of BMHVs, and it is also demonstrated by the flow through arteries (Causin et al., 2005; Degroote et al., 2008, 2010). It is concluded that relaxation can be used to obtain stable and efficient approximations for the subsequent angular accelerations of the valve leaflets. Several coupling schemes with relaxation have thus been developed, and they can be divided into loose and strong coupling schemes.

In the loose coupling methods, only one coupling iteration is needed in each time-step, since the solution of the flow field at time-step n is used to calculate the angular accelerations of the leaflets for the next time-step $n+1$:

$$\ddot{\theta}_i^{n+1} = \left(1 - \omega_i^{n+1}\right) \cdot \ddot{\theta}_i^n + \omega_i^{n+1} \cdot \frac{M_i^n}{I_i} \tag{8}$$

A relaxation factor ($\omega_i^{n+1} < 1$) is necessary, since the scheme without relaxation ($\omega_i^{n+1} = 1$) is unstable (Causin et al., 2005; Vierendeels et al., 2005; Borazjani et al., 2008), as mentioned above. The loose coupling formulation is often used to simulate heart valves (Redaelli et al., 2004; Morsi et al., 2007; Nobili et al., 2007; Tai et al., 2007; Borazjani et al., 2008; Xia et al., 2009). It has the main benefit of a low computational cost because of the lack of a coupling iteration loop within each time-step. However, this lack implies that dynamic equilibrium at the fluid-structure interface (Equation (6)) is not necessarily achieved, which leads to unphysical oscillations in the leaflet movement and the flow and pressure field, as described in Annerel et al. (2011).

Dynamic equilibrium at the fluid-structure interface can be obtained by introducing a coupling iteration loop within each time-step, as is the case in the strong coupling methods. Generally, each of the strong coupling iterations follows the same pattern, as visualized in Fig. 2. At the beginning of each coupling iteration k of time-step $n+1$, the motion of the leaflets is computed from the angular accelerations $\ddot{\theta}_i^{n+1,k}$. The mesh is moved and the flow equations are solved. From the flow field, the moments $M_i^{n+1,k}$ are calculated. Finally, the convergence of the dynamic equilibrium at the fluid-structure interface, expressed by Equation (6), is checked. When this dynamic equilibrium is obtained, a new time-step is initiated. However, when dynamic equilibrium is not achieved, a new coupling iteration $k+1$ is initiated, and thus new angular accelerations $\ddot{\theta}_i^{n+1,k+1}$ need to be calculated. Therefore, introducing a coupling iteration loop requires, in each coupling iteration k of time-step $n+1$, a stable and efficient approximation of the angular accelerations for the next coupling iteration $k+1$.
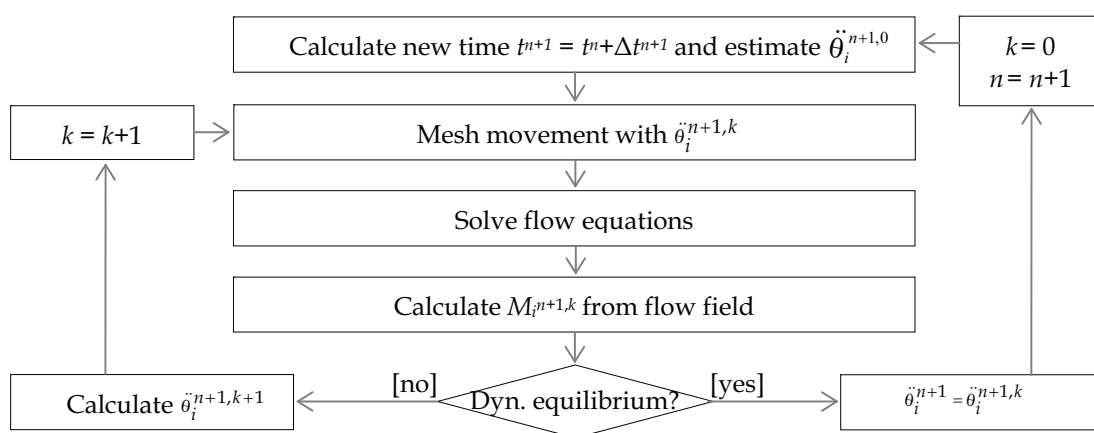

Fig. 2. Simplified flow chart of a strong FSI coupling algorithm with two degrees of freedom. n = time-step, k = coupling iteration step, i = leaflet number

A strong coupling scheme without relaxation can easily be proposed. From the moments of coupling iteration k in time-step $n+1$, the angular accelerations of the next coupling iteration $k+1$, i.e. $\ddot{\theta}_i^{n+1,k+1}$, can be calculated:

$$\ddot{\theta}_i^{n+1,k+1} = \frac{M_i^{n+1,k}}{I_i} \tag{9}$$

Unfortunately, such fixed-point iterations, also called Gauss-Seidel iterations without relaxation, are unstable for BMHVs (Vierendeels et al., 2005). Therefore, the scheme needs to be stabilized by using an appropriate prediction of the moments of the next coupling iteration $k+1$:

$$\ddot{\theta}_i^{n+1,k+1} = \frac{\hat{M}_i^{n+1,k+1}}{I_i} \tag{10}$$

with $\hat{M}_i^{n+1,k+1}$ denoting the predicted moment. Several methods are used in the literature to calculate a stable value for $\hat{M}_i^{n+1,k+1}$. Usually, this is achieved using a relaxation scheme, which leads to fixed-point iterations with relaxation ($\omega_i^{n+1,k} < 1$), also called the Gauss-Seidel coupling method with relaxation:

$$\hat{M}_i^{n+1,k+1} = \left(1 - \omega_i^{n+1,k}\right) \cdot I_i \ddot{\theta}_i^{n+1,k} + \omega_i^{n+1,k} \cdot M_i^{n+1,k} \tag{11}$$

Inserted in Equation (10):

$$\ddot{\theta}_i^{n+1,k+1} = \left(1 - \omega_i^{n+1,k}\right) \cdot \ddot{\theta}_i^{n+1,k} + \omega_i^{n+1,k} \cdot \frac{M_i^{n+1,k}}{I_i} \tag{12}$$

To simulate a BMHV in a partitioned way, several methods can be used to calculate an appropriate relaxation factor $\omega_i^{n+1,k}$ that stabilizes the solution process. In the following, using a fixed relaxation factor and a dynamic relaxation factor is discussed.

For the fixed relaxation factor, the factor value is kept constant during the entire simulation, as described in Le Tallec & Mouro (2001) for an industrial shock absorber valve:

$$\omega_i^{n+1,k} = \omega = Cst \tag{13}$$

Fixed relaxation was used to simulate the dynamics of a BMHV with a partitioned solver by Penrose et al. (2002), Nobili et al. (2007, 2008), Borazjani et al. (2008), De Tullio et al. (2009), and Hong et al. (2009). The main disadvantage of such a fixed relaxation is the lack of a physical meaning of the relaxation factor (Annerel et al., 2011). Therefore, the selection of an appropriate factor value is ad hoc and will be done primarily through trial-and-error, as noted by De Tullio et al. (2009).

For the dynamic relaxation factor, the factor value is updated in each coupling iteration of each time-step. Typically, the Aitken Δ^2 relaxation is used, as described in Irons et al. (1969), Mok et al. (2001), and Küttler et al. (2008). The Aitken Δ^2 relaxation updates the value of the factor in each coupling iteration of each time-step $n+1$:

$$\omega_i^{n+1,k} = \omega^{n+1,k} = -\frac{\left(\ddot{\theta}^{n+1,k} - \ddot{\theta}^{n+1,k-1}\right)^T \left(r^{n+1,k} - r^{n+1,k-1}\right)}{\left(r^{n+1,k} - r^{n+1,k-1}\right)^T \left(r^{n+1,k} - r^{n+1,k-1}\right)} \tag{14}$$

with

$$\ddot{\theta}^{n+1,k} = \begin{bmatrix} \ddot{\theta}_1^{n+1,k} \\ \ddot{\theta}_2^{n+1,k} \end{bmatrix} \quad \text{and} \quad r^{n+1,k} = \begin{bmatrix} \dfrac{M_1^{n+1,k}}{I_1} - \ddot{\theta}_1^{n+1,k} \\ \dfrac{M_2^{n+1,k}}{I_2} - \ddot{\theta}_2^{n+1,k} \end{bmatrix} \tag{15}$$

Partitioned simulations of heart valves using the Aitken Δ^2 relaxation method are reported in Borazjani et al. (2008), Diniz dos Santos et al. (2008), and Astorino et al. (2009).

More recently, however, a (quasi-Newton) method with a dynamically changing relaxation matrix has been developed (Annerel et al., 2010; Dahl et al., 2010) and subsequently optimized in Annerel et al. (2011). The method is an extension of Vierendeels et al. (2005) and predicts the moments of the next coupling iteration (i.e. $\hat{M}_i^{n+1,k+1}$ in Equation (10)) through a linearization of the dynamic equilibrium. Thus, while taking into account the mutual interaction between the leaflets, Equation (6) is linearized for each coupling iteration $k+1$ of time-step $n+1$:

$$\begin{cases} M_1^{n+1,k} + \left(\dfrac{\partial M_1}{\partial \ddot{\theta}_1}\right)^{n+1,k} \left(\ddot{\theta}_1^{n+1,k+1} - \ddot{\theta}_1^{n+1,k}\right) + \left(\dfrac{\partial M_1}{\partial \ddot{\theta}_2}\right)^{n+1,k} \left(\ddot{\theta}_2^{n+1,k+1} - \ddot{\theta}_2^{n+1,k}\right) = I_1 \cdot \ddot{\theta}_1^{n+1,k+1} \\[4mm] M_2^{n+1,k} + \left(\dfrac{\partial M_2}{\partial \ddot{\theta}_1}\right)^{n+1,k} \left(\ddot{\theta}_1^{n+1,k+1} - \ddot{\theta}_1^{n+1,k}\right) + \left(\dfrac{\partial M_2}{\partial \ddot{\theta}_2}\right)^{n+1,k} \left(\ddot{\theta}_2^{n+1,k+1} - \ddot{\theta}_2^{n+1,k}\right) = I_2 \cdot \ddot{\theta}_2^{n+1,k+1} \end{cases} \quad (16)$$

The components of the Jacobian are the derivatives of the moments (exerted by the flow on the leaflets) with respect to changes in leaflet angular accelerations. This Jacobian is approximated with finite differences and is numerically calculated from the flow solver by variations of the leaflet angular accelerations. This method outperforms the fixed relaxation and Aitken Δ^2 relaxation in needed coupling iterations per time-step and CPU time (Annerel et al., 2010, 2011).

3. Insights into the general dynamics and flow fields of an aortic BMHV

The dynamics of a BMHV depend on passive movement. Therefore, the opening and closure of the leaflets are governed by the pressure gradients and flow fields in the heart and arteries (in case of atrioventricular valves) (Butany et al., 2003).

In the following, the kinematics and dynamics of a BMHV are discussed and obtained by numerical simulations in an axisymmetric geometry (Yoganathan et al., 2004; Borazjani et al., 2008; De Tullio et al., 2009; Sotiropoulos et al., 2009) and verified by experiments (Dasi et al., 2007). These discussed dynamics are also illustrated in the numerical simulations done in Section 4.

Opening phase

The contraction of the left ventricle at the beginning of systole induces an increase of the left ventricular pressure. Because of the resulting positive transvalvular pressure gradient, the flow starts to accelerate and induces the opening of the valve.

In a BMHV, the valve leaflets initially open with a large increase in angular acceleration (and related angular velocity). However, as the valve opens, the leaflets tend to align with the axial flow, and their local linear velocity tends to become orthogonal to the main flow stream lines, which produces a pressure moment that decreases the angular acceleration and lowers the angular velocity (De Tullio et al., 2009). This deceleration is beneficial because it results in a very small angular velocity of the leaflets when the leaflets reach the fully open position; therefore, it significantly lowers the impact forces at the blocking mechanism.

During the early leaflet opening phase, three jet flows are formed, with the roll-up of the valve housing shear layer into the aortic sinuses of Valsalva and the formation of two shear layers shed from the tips of the valve leaflets (Borazjani et al., 2008; De Tullio et al., 2009; Sotiropoulos et al., 2009). Subsequently, these leaflet shear layers break down and large-scale von Karman-like vortex shedding emerges (Sotiropoulos et al., 2009).

Fully open position

When the leaflets have reached the fully open position, the flow rate continues increasing until its maximum value at peak systole. Due to the acceleration of the flow, the formation of small-scale turbulence is prevented, and the bulk of the flow remains laminar (De Tullio et al., 2009). However, at peak systole, the flow starts to decelerate. Subsequently, the large-scale vortices in the sinuses of Valsalva and the leaflet shear layers rapidly undergo the

transition to a small-scale turbulent state downstream of the valve (Borazjani et al., 2008; Sotiropoulos et al., 2009).

Closing phase

The valve leaflets start to close at the beginning of the steepest flow deceleration (De Tullio et al., 2009). Since the leaflets need to rotate over a large angle, some regurgitation occurs. The total volume of this reverse flow is denoted as the "closing volume" (as also described in Section 5).

During leaflet closure, the angular velocity of the leaflets keeps increasing until the closed position is reached. This gives rise to very large angular velocities (and thus stresses) when the leaflets impact the blocking mechanism at the fully closed position. Therefore, the closing kinematics are very different from those at the leaflet opening phase because the end of the opening occurs with small angular velocities, while at the end of the closing, the angular velocity attains peak value (De Tullio et al., 2009).

During the closing phase, the decelerating flow field is governed by small-scale eddies and turbulent vortices (Borazjani et al., 2008; Sotiropoulos et al., 2009).

Fully closed position

The leaflets reach the fully closed position at the negative peak of the flow rate (De Tullio et al., 2009). Due to the negative transvalvular pressure gradient when the leaflets are closed, flow leaks through the small gaps between the leaflets and through the gaps between the leaflets and valve casing (in particular, near the hinges), giving rise to squeezed jet flow. The total amount of this regurgitant flow is denoted as the "leakage volume" (see Section 5).

After valve closure, the turbulent structures in the flow slowly decay. Subsequently, the residual vortical structures are rapidly washed out at the beginning of a new cycle by the incoming accelerated flow when the valve reopens. (Borazjani et al., 2008; De Tullio et al., 2009; Sotiropoulos et al., 2009).

4. Three-dimensional strongly coupled partitioned FSI simulations of a BMHV

To illustrate the previous section, a BMHV is simulated in three different geometries. The used BMHV is a simplified model of the 25-mm ATS Open Pivot™ Standard Heart Valve in aortic position, with the orifice inner diameter measuring 20.8mm. The valve is simplified at the hinge regions by cutting away the blocking mechanism and hinges at the casing. Because of this simplification, the resulting opening velocity of the valve leaflets could become slightly overestimated since the additional counteracting moment created by the decelerated squeeze flows near the pivot hinge regions (i.e. the so-called pivot effect, as observed in the experiments in Feng et al. (1999)) is absent.

The valve is subsequently placed in three geometries. The first geometry consists of a rigid straight tube, as visualized in Fig. 3(*left*). The second geometry also consists of a rigid straight tube upstream of the valve, but rigid sinuses of Valsalva are added downstream of the valve. Such sinuses of Valsalva are anatomically present in the ascending aortic root and influence the valve closing (Grigioni et al., 2004). The sinuses of Valsalva are based on the geometry described in Reul et al. (1990) and are positioned symmetrically with respect to the leaflet rotation axes (Fig. 3(*middle*)). In the third geometry, the same sinuses of Valsalva are used, but they are placed asymmetrically (angle: 30°) with respect to the leaflet rotation axes in such a way that one of the leaflets directly faces one sinus (Fig. 3(*right*)).

For the geometries, the upstream tube has a diameter of 22mm and is 75mm long. The downstream geometry is 95mm long. The diameter of the downstream tube is 27.36 mm for the sinuses of Valsalva and 22mm for the straight tube.

These geometries are based on clinical practice, because when implanting the BMHV, the surgeon can choose to preserve the sinuses of Valsalva or to cut them away and replace the entire ascending aortic root (in the so-called Bentall procedure (Bentall et al., 1968)). Moreover, the surgeon can choose to position the valve symmetrically to the physiological sinuses of Valsalva, or to position it asymmetrically.

An unstructured fluid grid, consisting of approximately 800 000 tetrahedral cells, is generated in the geometries. Two cell layers are generated in the gap (which measures 0.1mm) between the leaflets and the casing near the hinge region. The ALE approach is followed, which means that the fluid grid follows the motion of the structure and subsequently needs an update to maintain good mesh quality. This update is done using a remeshing method and spring-based smoothing.
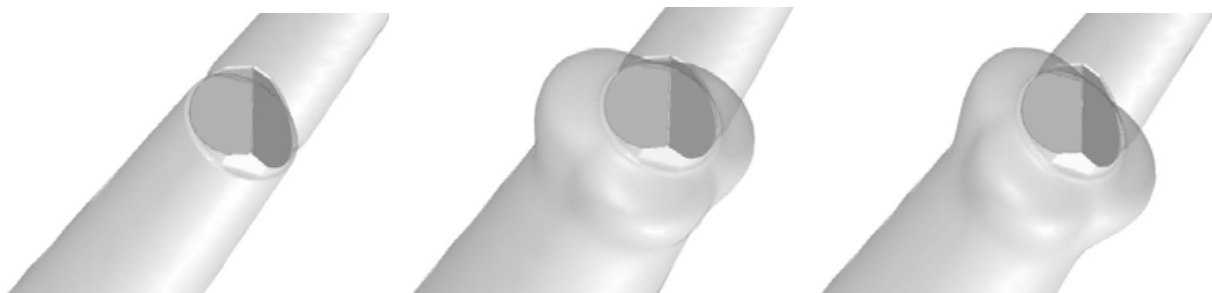

Fig. 3. Isometric view of the different geometries. *Left*: first geometry with straight tube. *Middle*: second geometry with symmetrically placed sinuses of Valsalva. *Right*: third geometry with asymmetrically positioned sinuses of Valsalva downstream of the valve

The dynamics of the BMHV are modeled by the strongly coupled partitioned quasi-Newton algorithm that was recently developed (Annerel et al., 2011). An inlet aortic flow pulse with a period of 1s (displayed in Fig. 4(*a*)) is imposed upstream and was previously used in Dumont et al. (2005, 2007) and Annerel et al. (2010, 2011). The flow pulse profile is uniform. A physiological pressure profile is imposed at the downstream outlet boundary. Note, however, that in a rigid geometry the pressure level does not affect the flow field since only the pressure gradient appears in the equations.

Blood is modeled as an incompressible Newtonian fluid with density and viscosity respectively equal to 1050kg/m³ and 4E-3Pa·s (i.e. the high shear rate limit viscosity of blood). Although real blood is a heterogeneous non-Newtonian fluid, the modeling of blood as a homogeneous Newtonian fluid for high shear rates is widely agreed upon for flow in large arteries and valves (Paul et al., 2003; Sotiropoulos et al., 2009). Nevertheless, it is important to keep in mind that when studying low levels of shear stresses, for example in the recirculation regions and vortices in the wake, the non-Newtonian effects could become important and should be taken into account when assessing the hemodynamics of the valve (Sotiropoulos et al., 2009). In such cases it is valuable to model the blood as a non-Newtonian fluid as in the Cross and Carreau model (Cross, 1965; Carreau, 1972). However, modeling of the fine-flow features and the hemodynamics is beyond the scope of the described simulations and, therefore, a Newtonian blood model is used.
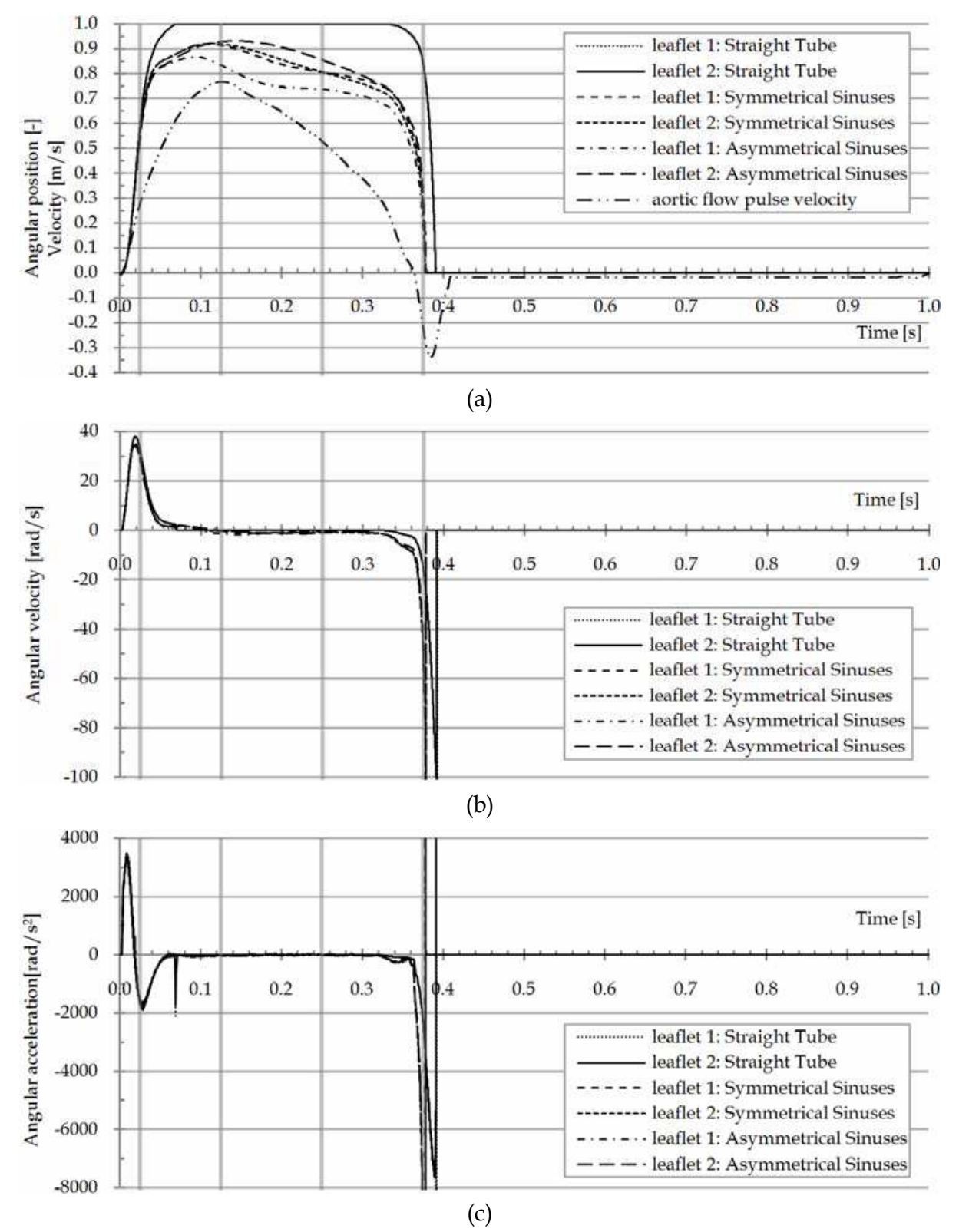
Fig. 4. Angular position of the leaflets (relative to maximal opening angle) and the aortic flow pulse velocity (*a*), angular velocity of the leaflets (*b*) and angular acceleration of the leaflets (*c*). The two leaflets of the geometry with the straight tube perform a complete symmetrical movement. The time levels at which the contours in Fig. 5 are shown are visualized by the vertical lines

No turbulence model is used, thus implying laminar flow. A no-slip boundary condition is applied at the walls. The valve is initially set in the closed position. The moment of inertia of one rigid valve leaflet about its rotation axis is equal to 9.94E-9kg·m².

The results of the simulations are depicted in Fig. 4 and Fig. 5. The angular positions of the leaflets are presented in Fig. 4(*a*), relative to the fully opened position. Therefore, 0 and 1 refer, respectively, to the fully closed and fully open position.

Although the valve leaflets open completely in the first geometry with the straight tube, the results show that this maximum opening position is not reached in both geometries with the sinuses of Valsalva. Such incomplete opening of the ATS Open Pivot™ Standard Heart Valve in a divergent geometry is explained by the greater sensitivity of the leaflet movement to the flow field compared with other BMHV designs, since the leaflets extend farther in the flow downstream of the orifice than is the case in other valve designs (Feng et al., 1999). Therefore, the valve does not open completely in the divergent transvalvular flow caused by the enlargement of the sinuses of Valsalva because the leaflets tend to align with the streamlines. In the straight tube, however, the valve leaflets open completely.

This incomplete opening also explains the difference in the closing phase between the geometries, since the valve in the sinuses of Valsalva geometries is closed sooner. This is because the leaflets in the straight tube reach the completely open position and therefore need to rotate over a greater angle in order to close. Hence, they have a greater closing volume (Feng et al., 2000). Nevertheless, the instant at which the leaflets start to close is approximately the same for both geometries.

Furthermore, for the asymmetrical geometry, the two leaflets show differences in movement. It can be understood that this asynchrony is triggered by the presence of the asymmetric geometry downstream of the valve (De Tullio et al., 2009; Hong et al., 2009). In the symmetrical geometries, there are no differences in movement between the two leaflets.

The velocity magnitudes at different time levels for the three geometries are shown in Fig. 5. Downstream of the valve, the three jet flows are clearly visible.

5. Design challenges

The ideal heart valve should have, among other things, a small drop in flow potential energy (i.e. small pressure drop over the valve and a high effective orifice area), a small retrograde flow, good hemodynamic properties, and high durability and safety in use.

In the remainder of this section, each of these design challenges will be discussed in detail.

Small regurgitation volume

Mechanical valves are characterized by a significant amount of regurgitant flow. This retrograde flow is the sum of the closing volume and the leakage flow (Yoganathan et al., 2004). The closing volume is the amount of reverse flow needed to let the leaflets rotate to the closed position. The leakage flow occurs during diastole, when the leaflets are in the closed position and blood flows back through the gaps of the valve due to the large negative pressure gradient over the valve.

The regurgitation volume V_{reg} (in ml) is typically measured by percentage (%reg) of forward stroke volume SV_{fwd} (in ml), as described in Verdonck et al. (2002):

$$\%reg = \frac{V_{reg}}{V_{reg} + SV_{fwd}} \tag{17}$$

Since the regurgitation lowers the net cardiac output and therefore enlarges the workload of the heart, its percentage should be minimized when designing heart valves.
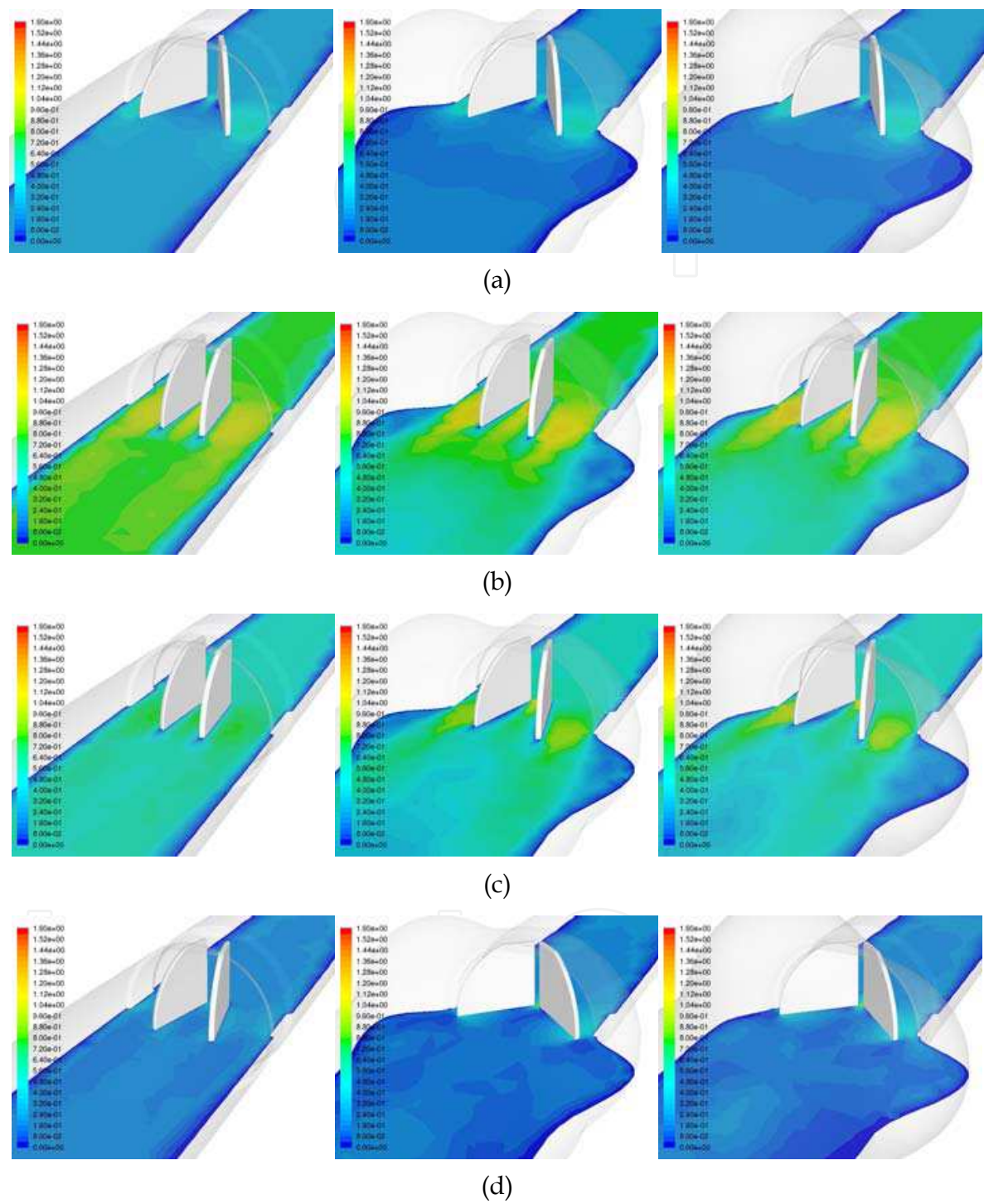

(a)

(b)

(c)

(d)

Fig. 5. Velocity Magnitude Contours in m/s visualized on a longitudinal section perpendicular to the leaflet rotation axes, for the geometry with the straight tube (*left*), the symmetrically placed sinuses of Valsalva (*middle*) and the asymmetrical sinuses of Valsalva (*right*). The plots are taken at *t* = 0.025s (*a*), *t* = 0.125s (*b*), *t* = 0.250s (*c*), and *t* = 0.375s (*d*), represented by the vertical lines in Fig. 4

Low transvalvular pressure gradient (TPG)

The transvalvular pressure gradient (TPG) is related to the drop in pressure that is needed for viscous blood to flow through the valve (Yoganathan et al., 2004). This forward pressure difference $\Delta p_{Doppler}$ (in mmHg) can be derived from a simplified form of the Bernoulli equation and the mean (Doppler) velocity V_{mean} (in m/s) during forward flow (Verdonck et al., 2002):

$$\Delta p_{Doppler} = 4V_{mean}^2 \tag{18}$$

The TPG is a measure of valve efficiency (Yoganathan et al., 2004). The workload on the left ventricle is directly related to the magnitude of this pressure difference, because when the magnitude of the TPG increases, an increasing systolic pressure in the left ventricle is needed to drive flow forward into the aorta. Therefore, the TPG should be minimized when designing valve prostheses (Yoganathan et al., 2004).

High effective orifice area (EOA)

Because the TPG is heavily dependent on the flow rate, another less flow-rate-dependent parameter is more commonly used as a measure for the quality of the valve, namely the effective orifice area (EOA).
Several formulations of the EOA (in cm²) can be defined, of which the Gorlin equation is mostly used (Baumgartner et al., 1992; Yoganathan et al., 1984). It is based on the fundamental hydraulic law of flow through an orifice and couples the flow through the valve orifice to the Doppler pressure gradient over the valve (Verdonck et al., 2002):

$$EOA = \frac{Q_{fwd,mean}}{51.6\sqrt{\Delta p_{Doppler}}} \tag{19}$$

where $Q_{fwd,mean}$ is the mean forward flow rate (in cm³/s). The constant 51.6 accounts for gravity and unit conversions (Baumgartner et al., 1992; Verdonck et al., 2002; Yoganathan et al., 2007).
The EOA is a measure for valve quality because it assesses the severity of the stenosis formed by the presence of the valve and thus the degree to which the prosthesis obstructs the blood flow (Yoganathan et al., 2004). A large EOA corresponds to a smaller pressure drop and thus to a smaller energy loss (Yoganathan et al., 2004). Therefore, when designing a valve prosthesis, the resulting EOA should be maximized.
Moreover, the EOA can be used to compare the efficiency of various valve designs, because it is a better index of valve function than is TPG alone (Zoghbi et al., 2009). However, to get a normalized value, the EOA should be made independent of the valve size by dividing it by the valve sewing ring area A_{sew}. This results in the performance index (PI), which provides a measure of the valve's resistance characteristics normalized to valve size (Yoganathan et al., 2004, 2007):

$$PI = \frac{EOA}{A_{sew}} \tag{20}$$

Therefore, the parameter PI can be used to fairly compare the efficiency of various artificial valves.

Good hemodynamic properties

One of the most challenging aspects in valve design is the improvement of hemocompatibility. Because the cardiovascular system is a closed circulatory system, damage to the blood cells can accumulate each time blood passes through the valve, which leads to an increased risk for platelet activation and hemolysis of the red blood cells (erythrocytes). This could result in clinical complications such as thromboembolisms and valve stenosis.

Blood cells can become damaged by non-physiological flow patterns or by contact with artificial materials (Paul et al., 2003). Therefore, to optimize blood flow through the valve, one should minimize the production of shear stresses and turbulence in the flow and avoid any flow stagnation and separation in the vicinity of the valve (Yoganathan et al., 2004). Moreover, the valve should be composed of (or coated with) biocompatible materials. Therefore, mostly pyrolytic carbon is used.

Durability and failure-safe design

Structural wear and fatigue of the valve can deteriorate the valve material and can cause severe valve failure.

Moreover, cavitation, which leads to erosion and pitting, can occur in BMHVs. Such cavitation-induced erosion and pitting were first related to BMHVs in the 1980s after observation of a series of severe leaflet escapes of the Edwards-Duromedics bileaflet valve (Mastroroberto et al., 2000; Johansen, 2004). It was seen that the hard, but brittle, pyrolytic carbon can become subject to cavitation-induced fatigue leading to a transverse fracture of the leaflet or a leaflet fracture near the pivot mechanism (Klepetko et al., 1989).

Later, leaflet escape in the same (but revised) bileaflet valve type was observed in mitral (Hemmer et al., 2000; Mert et al., 2003) and aortic position (Christiansen, 2001).

Therefore, for a durable and failure-safe design, the structural wear and fatigue potential should be minimized along with a minimization of the formation of cavitation bubbles.

Design challenges and BMHVs

Although current aortic BMHVs show a higher EOA and a higher PI compared with other artificial heart valve designs, such as the caged ball valve, the tilting disc valve, and the (non)stented bioprostheses (Yoganathan et al., 2004), some major design challenges concerning the hemodynamics and the durability need to be resolved. Moreover, BMHVs have a larger regurgitant volume than other artificial valves (Yoganathan et al., 2004).

In the remainder of this section, the hemodynamics and the cavitation of the BMHV are discussed in detail, with special interest to the flow near the hinges.

5.1 Blood damage and BMHVs

When blood flows through artificial devices, blood particulates can become damaged and initiate a cascade of events leading to coagulation and the formation of thrombi. Therefore, when a BMHV is implanted, the patient is required to take lifelong anticoagulation therapies (Paul et al., 2003; Bluestein et al., 2004; Dasi et al., 2009; Morbiducci et al., 2009).

Blood trauma can occur via several mechanisms, depending on the type of damaged blood cell. In the past, the fragmentation and damaging of erythrocytes was experimentally quantified, since this leads to hemolysis (Sutera et al., 1975; Paul et al., 2003). In recent years, however, platelet activation is believed to be the major underlying formation mechanism for thromboembolic complications in the flow past mechanical heart valves (Bluestein, 2004; Morbiducci et al., 2009).

The amount of blood damage depends primarily on the cumulative effect of the magnitude and the duration (the exposure time) of the applied force. Critical values of both factors can be exceeded by flow-dependent and non-flow-dependent causes (Paul et al., 2003).

The non-flow-dependent causes are the contact with artificial surfaces, which can be eliminated by using biocompatible materials. Therefore, pyrolytic carbon is commonly used for BMHVs because of its strength and high durability (Chandran et al., 2010) and good biocompatible properties (Johansen, 2004).

The flow-dependent causes are believed to originate from non-physiological flow patterns. However, despite many research efforts, the exact mechanisms underlying these flow-induced thromboembolic complications are still poorly understood (Bluestein, 2004). It is believed that the presence of elevated shear stresses in the flow is the most important platelet-damaging effect. Three non-physiological flow patterns can be distinguished.

Firstly, the squeeze flows observed as leakage flow when the leaflets are completely closed during diastole are of specific interest. Some leakage flow near the hinges is beneficial because it washes out the hinge regions and prevents flow stagnation and the development of thrombosis. However, the high-flow-velocity gradients can become too large, which causes elevated shear stresses and related platelet activation (Yoganathan et al., 2004).

Secondly, regions of flow separation, recirculation, and stagnation promote the deposition of damaged blood cells and increase the formation of thrombi (Yoganathan et al., 2004).

Finally, the shear layers surrounding the leaflets and the wake also expose the platelets to elevated shear stresses and lead them towards entrapment in the shed vortices of the wake (Bluestein et al., 2002).

Several studies used numerical methods to calculate the accumulated platelet activation when the blood flows through a BMHV. In the past, the valve leaflets were kept in a fixed position throughout the cardiac cycle due to the computational cost (Bluestein et al., 2002; Alemu et al., 2007; Dumont et al., 2005, 2007). More recently, however, Morbiducci et al. (2009) combined numerical FSI simulations with a numerical blood damage model. They reported that platelet activation is lower at early systole than at late systole and that the spanwise vorticity has a greater influence on the activation of platelets than does the streamwise vorticity.

A critical value for accumulated shear stress above which platelets are considered activated is, for example, given by the Hellums activation threshold criterion, i.e. $3.5 Ns/m^2$ (Hellums et al., 1987; Dumont et al., 2007).

5.2 Cavitation and BMHVs

Cavitation is the formation of voids or gas bubbles in liquids caused by a local reduction of the pressure to below that of vapor pressure. However, as soon as the surrounding pressure increases above vapor pressure, the formed bubbles will rapidly implode, which produces devastating shockwaves in the surrounding fluid (Johansen, 2004).

Several fluid mechanisms can lead to a pressure drop below vapor pressure in the blood flow during the closing phase of a BMHV. Firstly, squeeze flows are considered a contributing factor to the initation of cavitation. Such squeeze jets are formed at the very instant before leaflet closing, when the blood between the leaflets and valve casing is accelerated through the narrowing gap. This creates a high velocity jet flow with a large pressure gradient. The pressure can locally fall below vapor pressure, thus leading to cavitation (Bluestein et al., 1994; Johansen, 2004). Secondly, large vortices can be shed from the leaflet tips during the closing of the leaflets and during regurgitation. Towards the core of these vortices, the pressure decreases and the flow velocity increases. Therefore, the

conditions for cavitation can be reached in these vortex cores (Avrahami et al., 2000; Johansen, 2004). Finally, the formation of cavitation bubbles can also be augmented by the sudden stop of the valve leaflets as they impact the casing, often referred to as "water hammer cavitation"(Lee et al., 2002; Johansen, 2004).

It is believed that in BMHVs none of these mechanisms alone but solely their combined interaction can initiate and augment cavitation. Moreover, valves with very stiff leaflets, closing at high velocity and decelerating rapidly (due to the impact at the blocking mechanism of the casing), are more prone to cause cavitation than valves with flexible leaflets that are gently decelerated (Zapanta et al., 1998; Johansen, 2004).

Although the formation of cavitation bubbles in the blood flow through a BMHV is an extremely rare phenomenon, it is undesirable because the shockwaves produced during the implosion of the cavitation bubbles can create high-velocity microjets. These microjets can deteriorate the valve structures as well as the nearby blood cells, thus leading to severe thromboembolic complications and valve failures (Johansen, 2004).

Cavitation-induced material deterioration of a BMHV was first related to BMHVs in the 1980s after several leaflet escapes of the Edwards-Duromedics bileaflet valve, as described above (Mastroroberto et al., 2000; Johansen, 2004). It was observed that the impingement of high-velocity microjets can cause erosion and pitting when it impacts the structural surfaces. Lee et al. (2002) reported the appearance of cavitation-induced erosion pits in regions where squeeze flow occurred immediately before valve closure. Moreover, the study indicated that the number of pits was closely related to the magnitude of the pressure drop caused by the water hammer phenomenon.

6. Conclusion

Each year, replacing failing aortic heart valves with mechanical heart valves saves thousands of human lives.

However, modern BMHVs are still far from perfect and still face major design challenges. Most of these design challenges involve the hemodynamic properties of the valve and are thus directly related to the blood flow. Therefore, a thorough understanding of the blood flow is required for design optimization.

Current numerical simulation techniques can provide such valuable information and are considered crucial for gaining insights into the blood flow and assessing the performance of future valve prototypes.

The numerical simulations discussed in this chapter illustrate the incomplete opening of the aortic ATS Open Pivot™ Standard Heart Valve in a diverging geometry. Moreover, asymmetrically placed sinuses of Valsalva induce an asymmetrical movement of the valve leaflets.

7. Acknowledgment

8. References

Akutsu, T. & Higuchi, D. (2001). Flow analysis of the bileaflet mechanical prosthetic heart valves using laser Doppler anemometer: effect of the valve designs and installed

orientations to the flow inside the simulated left ventricle. *J Artif Organs*, Vol. 4, pp. 113-125.

Alemu, Y. & Bluestein, D. (2007). Flow-induced platelet activation and damage accumulation in a mechanical heart valve: numerical studies. *Artific Organs*, Vol. 31, No. 9, pp. 677-688.

Aljassim, O., Svensson, G., Houltz, E. & Bech-Hanssen, O. (2008). Doppler-catheter discrepancies in patients with bileaflet mechanical prostheses or bioprostheses in the aortic valve position. *Am J Cardiol*, Vol. 2008, pp. 1383-1389.

Annerel, S., Degroote, J., Claessens, T. & Vierendeels, J. (2010). Evaluation of a new implicit coupling algorithm for the partitioned fluid-structure interaction simulation of bileaflet mechanical heart valves. *IOP Conf Ser: Mater Sci Eng*, Vol. 10, 012124.

Annerel, S., Degroote, J., Claessens, T., *et al.* (2011). A fast strong coupling algorithm for the partitioned fluid-structure interaction simulation of BMHVs. *Comput Method Biomec*, In press.

Aoyagi, S., Arinaga, K., Fukunaga, S., Tayama, E., Kosuga, T. & Akashi, H. (2006). Leaflet movement of the ATS Valve in the aortic position: unique behavior observed in 19-mm valves. *Ann Thorac Surg*, Vol. 82, pp. 853-857.

Aslam, A.K., Aslam, A.F., Vasavada, B. & Khan, I.A. (2007). Prosthetic heart valves: types and echocardiographic evaluation. *Int J Cardiol*, Vol. 122, pp. 99-110.

Astorino, M., Gerbeau, J.-F., Pantz, O. & Traoré, K.-F. (2009). Fluid-structure interaction and multi-body contact: application to aortic valves. *Comput Methods Appl Mech Engrg*, Vol. 198, pp. 3603-3612.

Avrahami, I., Rosenfeld, M., Einav, S., Eichler, M. & Reul, H. (2000). Can vortices in the flow across mechanical heart valves contribute to cavitation? *Med Biol Eng Comput*, Vol. 38, pp. 93-97.

Bang, J.S., Yoo, S.M. & Kim, C.N. (2006). Characteristics of pulsatile blood flow through the curved bileaflet mechanical heart valve installed in two different types of blood vessels: velocity and pressure of blood flow. *ASAIO J*, Vol. 52, pp. 234-242.

Baumgartner, H., Khan, S.S., DeRobertis, M., Czer, L.S. & Maurer, G. (1992). Doppler assessment of prosthetic valve orifice area. An in vitro study. *Circulation*, Vol. 85, pp. 2275-2283.

Bech-Hanssen, O., Caidahl, K., Wallentin, I., Ask, P. & Wranne, B. (2001). Assessment of effective orifice area of prosthetic aortic valves with Doppler echocardiography: An in vivo and in vitro study. *J Thorac Cardiovasc Surg*, Vol. 122, pp. 287-295.

Bentall, H. & De Bono, A. (1968). A technique for complete replacement of the ascending aorta. *Thorax*, Vol. 23, pp. 338-339.

Bluestein, D., Einav, S. & Hwang, N.H.C. (1994). A squeeze flow phenomenon at the closing of a bileaflet mechanical heart valve prosthesis. *J Biomech*, Vol. 27, No. 11, pp. 1369-1378.

Bluestein, D., Li, Y.M. & Krukenkamp, I.B. (2002). Free emboli formation in the wake of bi-leaflet mechanical heart valves and the effects of implantation techniques. *J Biomech*, Vol. 35, pp. 1533-1540.

Bluestein, D. (2004). Research approaches for studying flow-induced thromboembolic complications in blood recirculating devices. *Expert Rev. Med Devices*, Vol. 1, No. 1, pp. 65-80.

Borazjani, I., Ge, L. & Sotiropoulos, F. (2008). Curvilinear immersed boundary method for simulating fluid structure interaction with complex 3D rigid bodies. *J Comput Phys*, Vol. 227, No. 16, pp. 7587-7620.

Browne, P., Ramuzat, A., Saxena, R. & Yoganathan, A.P. (2000). Experimental investigation of the steady flow downstream of the St. Jude bileaflet heart valve: A comparison between laser Doppler velocimetry and particle image velocimetry techniques. *Ann Biomed Eng*, Vol. 28, No. 1, pp. 39-47.

Butany, J., Ahluwalia, M.S., Munroe, C., *et al.* (2003). Mechanical heart valve prostheses: identification and evaluation (erratum). *Cardiovasc Pathol*, Vol. 12, pp. 322-344.

Carreau, P. (1972). Rheological equations from molecular network theories. *Trans Soc Rheol*, Vol. 16, No.1, pp. 99–127.

Causin, P., Gerbeau, J.-F. & Nobile, F. (2005). Added-mass effect in the design of partitioned algorithms for fluid-structure problems. *Comput Methods Appl Mech Engrg*, Vol. 194, pp. 4506-4527.

Choi, C.R. & Kim, C.N. (2009). Numerical analysis on the hemodynamics and leaflet dynamics in a bileaflet mechanical heart valve using a fluid-structure interaction method. *ASAIO J*, Vol. 55, No. 5, pp. 428-437.

Christiansen, S., Scheld, H.H. & Hammel, D. (2001). Leaflet escape in a Tekna valve in aortic position. *Ann Thorac Surg*, Vol. 71, p. 761.

Cross, M. (1965). Rheology of non-Newtonian fluids: a new flow equation for pseudoplastic systems. *J Colloid*, Vol. 20, pp. 417–437.

Dahl, S.K., Vierendeels, J., Degroote, J., Annerel, S., Hellevik, L.R. & Skallerud, B. (2010). FSI-simulation of asymmetric mitral valve dynamics during diastolic filling. *Comput Method Biomec*, DOI: 10.1080/10255842.2010.517200.

Dasi, L.P., Ge, L., Simon, H.A., Sotiropoulos, F. & Yoganathan, A.P. (2007). Vorticity dynamics of a bileaflet mechanical heart valve in an axisymmetric aorta. *Phys Fluids*, Vol. 19, 067105.

Dasi, L.P., Simon, H.A., Sucosky, P. & Yoganathan, A.P. (2009). Fluid mechanics of artificial heart valves. *Clin Exp Pharmacol Physiol*, Vol. 36, pp. 225-237.

Degroote, J., Bruggeman, P., Haelterman, R. & Vierendeels, J. (2008). Stability of a coupling technique for partitioned solvers in FSI applications. *Comput Struct*, Vol. 86, pp. 2224-2234.

Degroote, J., Annerel, S. & Vierendeels, J. (2010). Stability analysis of Gauss-Seidel iterations in a partitioned simulation of fluid-structure interaction. *Comput Struct*, Vol. 88, pp. 263-271.

De Hart, J., Peters, G.W.M., Schreurs, P.J.G. & Baaijens, F.P.T. (2000). A two-dimensional flui-structure interaction model of the aortic value. *J Biomech*, Vol. 33, pp. 1079-1088.

De Hart, J., Peters, G.W.M., Schreurs, P.J.G. & Baaijens, F.P.T. (2003). A three-dimensional computational analysis of fluid–structure interaction in the aortic valve. *J Biomech*, Vol. 36, pp. 103–112.

De Tullio, M.D., Cristallo, A., Balaras, E. & Verzicco, R. (2009). Direct numerical simulation of the pulsatile flow through an aortic bileaflet mechanical heart valve. *J Fluid Mech*, Vol. 622, pp. 259-290.

Diniz dos Santos, N.D., Gerbeau, J.-F. & Bourgat, J.-F. (2008). A partitioned fluid-structure algorithm for elastic thin valves with contact. *Comput Methods Appl Mech Engrg*, Vol. 197, pp. 1750-1761.

Donea, J., Huerta, A., Ponthot, J.-P. & Ferran A.R. (2004). Chapter 14 Arbitrary Lagrangian-Eulerian Methods, In: *Encyclopedia of Computational Mechanics, Volume 1: Fundamentals*. E. Stein, R. de Borst, J.R. Hughes (Eds.), John Wiley & Sons, ISBN:0-470-84699-2.

Dumont, K., Segers, P., Vandenberghe, S., Van Nooten, G. & Verdonck, R. (2002). Omnicarbon 21 mm aortic valve prosthesis: in vitro hydrodynamic and echo-doppler study. *Int J Artif Organs*, Vol. 25, pp. 783-790.

Dumont, K., Vierendeels, J., Segers, P., Van Nooten, G. & Verdonck, P. (2005). Predicting ATS Open Pivot Heart Valve performance with computational fluid dynamic. *J Heart Valve Dis*, Vol. 14, pp. 393-399.

Dumont, K., Vierendeels, J., Kaminsky, R., Van Nooten, G., Verdonck, P. & Bluestein, D. (2007). Comparison of the hemodynamic and thrombogenic performance of two bileaflet mechanical heart valves using a CFD/FSI model. *J Biomech Eng*, Vol. 129, pp. 558-565.

Feng, Z., Umezu, M., Fujimoto, T., *et al*. (1999). Analysis of ATS leaflet behaviour by in vitro experiment. *J Artif Organs*, Vol. 2, pp. 46-52.

Feng, Z., Umezu, M., Fujimoto, T., Tsukahara, T., Nurishi, M. & Kawaguchi, D. (2000). In vitro hydrodynamic characteristics among three bileaflet valves in the mitral position. *J Artif Organs*, Vol. 24, No. 5, pp. 346-352.

Feng, Z., Nakamura, T., Fujimoto, T. & Umezu, M. (2001). Influence of valve size on the hydrodynamic performance of the ATS valve. *J Artif Organs*, Vol. 4, pp. 303-307.

Grigioni, M., Daniele, C., D'Avenio, G., *et al*. (2004). Innovative technologies for the assessment of cardiovascular medical devices: state-of-the-art techniques for artificial heart valve testing. *Expert Rev Med Devices*, Vol. 1, No. 1, pp. 81-93.

Guivier, C., Deplano, V. & Pibarot, P. (2007). New insights into the assessment of the prosthetic valve performance in the presence of subaortic stenosis through a fluid-structure interaction model. *J Biomech*, Vol. 40, pp. 2283-2290.

Guivier-Curien, C., Deplano, V. & Bertrand, E. (2009). Validation of a numerical 3-D fluid-structure interaction model for a prosthetic valve based on experimental PIV measurements. *Med Eng Phys*, Vol. 31, pp. 986-993.

Hellums, J., Peterson, D., Stathopoulos, N., Moake, J. & Giorgio, T. (1987). Studies on the mechanisms of shear-induced platelet activation, Springer-Verlag, New York.

Hemmer, W.B., Doss, M., Hannekum, A. & Kapfer, X. (2000). Leaflet escape in a TEKNA and an original duromedics bileaflet valve. *Ann Thorac Surg*, Vol. 69, pp. 942-944.

Hirt, C.W., Amsden, A.A. & Cook, J.L. (1997). An arbitrary Lagrangian-Eulerian computing method for all flow speeds. *J Comput Phys*, Vol. 135, pp. 203-216.

Hufnagel, C.A., Harvey, W.P., Rabil, P.J. & McDermott, T.F. (1954). Surgical correction of aortic insufficiency. *Surgery*, Vol. 35, pp. 673–683.

Irons, B.M. & Tuck, R.C. (1969). A version of the Aitken accelerator for computer iteration. *Int J Numer Meth Eng*, Vol. 1, pp. 275-277.

Johansen, P. (2004). Mechanical heart valve cavitation. *Expert Rev Med Devices*, Vol. 1, No. 1, pp. 95-104.

Kaminsky, R., Kallweit, S., Weber, H.-J., Claessens, T., Jozwik, K. & Verdonck, P. (2007). Flow visualization through two types of aortic prosthetic heart valves using stereoscopic high-speed particle image velocimetry. *Artif Organs*, Vol. 31, No. 12, pp. 869-879.

Kelly, S., Verdonck, P., Vierendeels, J., Riemslagh, K., Dick, E. & Van Nooten, G. (1999). A three-dimensional analysis of flow in the pivot regions of an ATS bileaflet valve. *Int J Artif Organs*, Vol. 22, pp. 754-763.

Klepetko, W., Moritz, A., Mlczoch, J., Schurawitzki, H., Domanig, E. & Wolner, E. (1989). Leaflet fracture in Edwards-Duromedics bileaflet valves. *J Thorac Cardiovasc Surg*, Vol. 97, No. 1, pp. 90-94.

Küttler, U. & Wall, W.A. (2008). Fixed-point fluid-structure interaction solvers with dynamic relaxation. *Comput Mech*, Vol. 43, pp. 61-72.

Lee, H., Yamamoto, K., Kudo, N., Shimooka, T., Mitamura, Y. & Yuhta, T. (2002). Examination of cavitation-induced surface erosion pitting of a mechanical heart valve using closing velocities. *J Artif Organs*, Vol. 5, pp. 193–199.

Le Tallec, P. & Mouro, J. (2001). Fluid structure interaction with large structural displacements. *Comput Methods Appl Mech Engrg*, Vol. 190, pp. 3039-3067.

Makhijani, V.B., Yang, H.Q., Dionne, P.J. & Thubrikar, M.J. (1997). Three-dimensional coupled fluid–structure simulation of pericardial bioprosthetic aortic valve function. *ASAIO J*, Vol. 43, No. 5, pp. M387–M392.

Masson, C. & Rieu, R. (1998). Time-frequency analysis of the noise produced by the closing of artificial heart valves: an in vitro study. *Med Eng Phys*, Vol. 20, pp. 418-431.

Mastroroberto, P., Chello, M., Bevacqua, E., Cirillo, F. & Covino, E. (2000). Duromedics original prosthesis: what do we really know about diagnosis and mechanism of leaflet escape? *Can J Cardiol*, Vol. 16, No. 10, pp. 1269-1272.

Mert, K., Ozkara, A. & Hatemi, A. (2003). Leaflet escape in a revised Edwards-Duromedics mitral prosthesis. *J Heart Valve Dis*, Vol. 12, No. 4, pp. 513-515.

Mok, D.P., Wall, W.A. & Ramm, E. (2001). Accelerated iterative substructuring schemes for instationary fluid-structure interaction. In: *Computational Fluid and Solid Mechanics*, K. Bathe (Ed.), Elsevier, pp. 1325-1328.

Morbiducci, U., Ponzini, R., Nobili, M., *et al*. (2009). Blood damage safety of prosthetic heart valves. Shear-induced platelet activation and local flow dynamics: a fluid-structure approach. *J Biomech*, Vol. 42, pp. 1952-1960.

Morsi, Y.S., Yang, W.W., Wong, C.S. & Das, S. (2007). Transient fluid-structure coupling for simulation of a trileaflet heart valve using weak coupling. *J Artif Organs*, Vol. 10, pp. 96-103.

Nobili, M., Passoni, G. & Redaelli, A. (2007). Two fluid-structure approaches for 3D simulation of St. Jude Medical bileaflet valve opening. *J Appl Biomater Biom*, Vol. 5, pp. 49-59.

Nobili, M., Morbiducci, U., Ponzini, R., *et al*. (2008). Numerical simulation of the dynamics of a bileaflet prosthetic heart valve using a fluid-structure interaction approaches. *J Biomech*, Vol. 41, pp. 2539-2550.

Paul, R., Apel, J., Klaus, S., Schügner, F., Schwindke, P. & Reul, H. (2003). Shear stress related blood damage in laminar Couette flow. *Artif Organs*, Vol. 27, No. 6, pp. 517-529.

Penrose, J.M.T. & Staples, C.J. (2002). Implicit fluid-structure coupling for simulation of cardiovascular problems. *Int J Numer Meth Fl*, Vol. 40, pp. 467-478.

Peskin, C. (1972). Flow patterns around heart valves: a numerical method. *J Comput Phys*, Vol. 10, pp. 252-271.

Redaelli, A., Bothorel, H., Votta, E., *et al*. (2004). 3-D Simulation of the St. Jude medical bileaflet valve opening process: fluid-structure interaction study and experimental validation. *J Heart Valve Dis*, Vol. 13, pp. 804-813.

Reul, H., Vahlbruch, A., Giersiepen, M., Schmitz-Rode, Th., Hirtz, V. & Effert, S. (1990). The geometry of the aortic root in health, at valve disease and after valve replacement. *J Biomech*, Vol. 23, pp. 181-191.

Sezai, A., Umeda, T., Hata, M., *et al*. (2009). A transesophageal echocardiographic and cine-fluoroscopic evaluation of an ATS prosthetic valve opening. *Surg Today*, Vol. 39, pp. 300-305.

Sotiropoulos, F. & Borazjani, I. (2009). A review of state-of-the-art numerical methods for simulating flow through mechanical heart valves. *Med Biol Eng Comput*, Vol. 47, pp. 245-256.

Sutera, S.P. & Mehrjardi, M.H. (1975). Deformation and fragmentation of human red blood cells in turbulent shear flow. *Biophys J*, Vol. 15, pp. 1-10.

Tai, C.H., Liew, K.M. & Zhao, Y. (2007). Numerical simulation of 3D fluid-structure interaction flow using an immersed object method with overlapping grid, *Comput Struct*, Vol. 85, pp. 749-762.

Van Loon, R., Anderson, P.D., de Hart, J. & Baaijens, F.P.T. (2004). A combined fictitious domain/adaptive meshing method for fluid-structure interaction in heart valves. *Int J Numer Meth Fl*, Vol. 46, pp. 533-544.

Verdonck, P. (2002). The role of computational fluid dynamics for artificial organ design. *Artif Organs*, Vol. 26, pp. 569-570.

Verdonck, P., Dumont, K., Segers, P., Vandenberghe, S. & Van Nooten, G. (2002). Mock loop testing of On-X prosthetic mitral valve with Doppler echocardiography. *Artif Organs*, Vol. 26, pp. 872-878.

Vierendeels, J., Dumont, K., Dick, E. & Verdonck, P. (2005). Analysis and stabilization of fluid-structure interaction algorithm for rigid-body motion. *AIAA J*, Vol. 43, pp. 2549-2557.

Vierendeels, J., Dumont, K. & Verdonck, P. (2008). A partitioned strongly coupled fluid-structure interaction method to model heart valve dynamics. *J Comput Appl Math*, Vol. 215, pp. 602-609.

Xia G.H., Zhao, Y. & Yeo, J.H. (2009). Parallel unstructured multigrid simulation of 3D unsteady flows and fluid-structure interaction in mechanical heart valve using immersed membrane method. *Comput Fluids*, Vol. 38, No. 1, pp. 71-79.

Yin, W., Krukenkamp, I.B., Saltman, A.E., *et al*. (2006). Thrombogenic performance of a St.Jude bileaflet mechanical heart valve in a sheep model. *ASAIO J*, Vol. 52, pp. 28-33.

Yoganathan, A.P., Chaux, A., Gray, R., *et al*. (1985). Bileaflet, tilting disc and porcine aortic valve substitutes: in vitro hydrodynamic characteristics. *J Am Coll Cardiol*, 3 Vol. 3, No. 2, pp. 313-320.

Yoganathan, A.P., He, Z. & Jones, S.C. (2004). Fluid mechanics of heart valves. *Annu Rev Biomed Eng*, Vol. 6, pp. 331-362.

Yoganathan, A.P., Chandran, K.B. & Sotiropoulos, F. (2005). Flow in prosthetic heart valves: state-of-the-art and future directions. *Ann Biomed Eng,*. Vol. 33, No. 12, pp. 1689-1694.

Yoganathan, A.P. & Travis, B.R. (2007). Chapter 24 Fluid dynamics of prosthetic valves, In: *The Practice of Clinical Echocardiography*, Third Edition, Otto C.M., Saunders Elsevier, ISBN: 978-1-4160-3640-1, pp. 552-577.

Zapanta, C.M., Stinebring, D.R., Deutsch, S., Geselowitz, D.B. & Tarbell, J.M. (1998). A comparison of the cavitation potential of prosthetic heart valves based on valve closing dynamics. *J Heart Valve Dis*, Vol. 7, No. 6, pp. 655-667.

Zoghbi, W.A., Chambers, J.B., Dumesnil, J.G., *et al*. (2009). Recommendations for evaluation of prosthetic valves with echocardiography and Doppler ultrasound. *J Am Soc Echocardiogr*, Vol. 22, No. 9, pp. 975–1014.
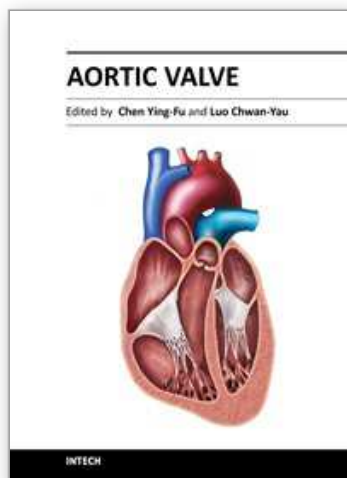
Aortic Valve

Edited by Prof. Chen Ying-Fu

Much has evolved in the field of aortic valve disease because of the increase in knowledge in the last decade, especially in the area of its management. This book "Aortic Valve" is comprised of 18 chapters covering basic science, general consideration of aortic valve disease, infective endocarditis, aortic sclerosis and aortic stenosis, bioprosthetic valve, transcatheter aortic valve implantation and a special section on congenital anomalies of the aortic valve. We hope this book will be particularly useful to cardiologists and cardiovascular surgeons and trainees. We also believe that this book will be a valuable resource for radiologists, pathologists, cardiovascular anesthesiologists, and other healthcare professionals who have a special interest in treating patients with aortic valve disease. We are certain that information in this book will help to provide virtually most new areas of aortic valve disease that will be employed in the current era.

How to reference

In order to correctly reference this scholarly work, feel free to copy and paste the following:

Sebastiaan Annerel, Tom Claessens, Peter Van Ransbeeck, Patrick Segers, Pascal Verdonck and Jan Vierendeels (2011). State-Of-The-Art Methods for the Numerical Simulation of Aortic BMHVs, Aortic Valve, Prof. Chen Ying-Fu (Ed.), ISBN: 978-953-307-561-7, InTech, Available from: http://www.intechopen.com/books/aortic-valve/state-of-the-art-methods-for-the-numerical-simulation-of-aortic-bmhvs

INTECH

open science | open minds